Department of Veterans Affairs

Journal of Rehabilitation Research and Development
Vol. 38 No. 4, July/August 2001
Pages 409–421

# Analysis of vibrations induced during wheelchair propulsion

**David P. VanSickle, PhD; Rory A. Cooper, PhD; Michael L. Boninger, MD; Carmen P. DiGiovine, MS**
*Human Engineering Research Laboratories, VA Rehabilitation Research and Development Center, VA Pittsburgh Healthcare System, Pittsburgh, PA; Departments of Rehabilitation Science & Technology, Physical Medicine & Rehabilitation, Mechanical Engineering, and Bioengineering, University of Pittsburgh, Pittsburgh, PA*

**Abstract—**Little is known about how dynamic acceleration affects wheelchair-rider comfort. The current study was to test both the operation of an instrumented wheelchair by a wheelchair user over a Simulated Road Course (SRC) and the operation of the same instrumented wheelchair during normal daily activities (a field test) by test subjects. Sixteen subjects participated in the protocol. A SRC allowed collection of data from wheelchair users traversing obstacles similar to those experienced by a typical wheelchair user. The SRC consisted of eight obstacles fixed rigidly to a flat concrete surface. The field test began after the conclusion of the SRC test. Transfer functions were derived for all 16 subjects. It is clear from the results that for the SRC, the acceleration at the wheelchair frame exceeded the 8-h "fatigue-decreased performance boundary." A vertical acceleration resonant peak was evident for eight of the subjects. The average for these peaks, when present, was 8.1 Hz. This frequency is higher than the 4–6 Hz resonant peak presented in the literature for a seated human subject. This discrepancy could be due to different levels of trunk control between wheelchair users in this study and ambulatory subjects used in the literature. Subjects and their wheelchairs were exposed to a few, high-acceleration events rather than consistent, small-magnitude accelerations during the field test. This study indicates that vibration may be a contributing factor to fatigue among manual wheelchair users, which could lead to injury.

**Key words:** *accelerations, design, instrumentation, modeling, vibrations, wheelchairs.*

## INTRODUCTION

A barrier to performing in-depth analyses during the processes of wheelchair design and "ride comfort assurance" is a lack of wheelchair-acceleration data, measured over time, that vary with the activity of the wheelchair rider. Furthermore, little is known about how this dynamic acceleration affects rider comfort. Most current literature focuses on the vibration exposure of a seated occupant. To this end, standards have been developed by the International Organization for Standardization (ISO) to quantify how much exposure is allowable for various frequencies of exposure.

This study attempts to apply current vibration standards to wheelchair users, with the purpose of achieving three goals: first, the development of instrumentation and techniques necessary to measure dynamic acceleration; second, the determination of potential health problems for wheelchair users, via current analytical techniques; and third, the determination of how well current

**This material is based upon work supported by the U.S. Department of Veterans Affairs, Veterans Health Administration, Rehabilitation Research and Development Service (B805-RA).**

Address all correspondence and requests for reprints to Rory A. Cooper, PhD, Human Engineering Research Laboratories (151-R1), Center of Excellence for Wheelchairs and Related Technology, VA Pittsburgh Healthcare System, 7180 Highland Drive, Pittsburgh, PA 15206; email: rcooper+@pitt.edu.

acceleration-analysis techniques apply to wheelchair users, based on their patterns of use. To achieve these goals, the current study was designed with multiple components. Two test situations were devised. One test was the operation of an instrumented wheelchair over a Simulated Road Course (SRC) and the other was the operation of the same, instrumented wheelchair during the normal daily activities of the test subjects.

Very few studies have been performed specifically to look at how dynamic acceleration affects wheelchair users. VanSickle and colleagues determined the acceleration of the rider on the American National Standards Institute/Rehabilitation Engineering Society of North America (ANSI/RESNA) standard Curb-Drop machine using an ANSI/RESNA test dummy (1,2). Using rigid-body dynamics, they were able to determine the acceleration at any point along the back and lap. The focus of that study was the determination of structural loads, however, and not rider comfort.

Other studies have focused on physiological parameters. Seidel, Bluethner, and Hinz (3) attempted to predict the compressive forces on the lumbar spine using electromyography and a model of the torso. Acceleration was measured at the head (with the use of a bite bar), shoulder, and the upper trunk. The combination of the accelerometer data with the predicted force applied by the back muscles was used to determine the compressive load. An interesting conclusion of the Seidel, Bluethner, and Hinz study was that the musculature of the back plays an active part in the resonant frequencies of the body (3). In contrast to those conclusions, Seroussi, Wilder, and Pope (4) found no evidence that the muscle activity played an important role in resonance. Their findings indicated that body resonance is due primarily to rocking at the pelvis and the resonance phenomenon has been shown in postures with low activity of the erector spinae muscles.

This present study focuses specifically on the influence of active and dynamic trunk control on whole-body resonance. In a radiographic study by Dupuis (5), resonance of the body was associated with an increase in the movement of the digestive organs. A meal enriched with Unibaryt C (a consumable barium-containing compound) was given to fourteen test subjects. Each of these test subjects underwent whole-body vibration for each of the three orthogonal directions (x,y,z) in the seated, standing, and reclining positions. The resonances of the shoulder, head, spinal column, and trunk were reported. In the vertical direction (z), all the body parts, with the exception of the head, had a resonance range centering at approximately 4 Hz.

Instead of using empirical methods, other investigators have attempted to use analytical modeling methods. Fairley and Griffin (6) presented one of the simplest models of the seated human. Their model contains only one parameter, which they term “the apparent mass.” In contrast, Muksian, and Nash (7) presented a 14 degree-of-freedom model for the seated person. In their model, the head, torso, thorax, back, diaphragm, abdomen, and legs are modeled as separate masses joined by spring-dampers units. The dampers of this model have a non-linear cubic relationship in order to obtain a good fit with published data. An attempt by Muksian and Nash (8) to reduce the number of degrees-of-freedom to three, while retaining the cubic dampening, failed to achieve acceptable results.

Amirouche (9) presented a model that divided the human body into an arbitrary number of segments. His model was simplified significantly by eliminating all degrees-of-freedom except vertical translation. After some empirical adjustments, the model did fit the data for seated vibration transmittance to the head. Amirouche, Xie, and Patwardhan (10) later used a similar model to optimize the characteristics of the contact between the vibrating surface and the human by minimizing the energy of body displacement.

The great variety of methods used underscores the need to develop systematically the instrumentation, measurement techniques, and analytical tools to accurately correlate dynamic acceleration with wheelchair comfort and possibly reduce associated health risks.

## METHODS

### Standard For Vibration Testing: ISO-2631

To standardize the methods of data collection for whole-body vibration, the ISO introduced the ISO-2631 (11,12). ISO-2631 specifies acceptable boundaries for vibration transmitted to the body in the seated and standing positions and is used in this study to analyze vibration data recorded from a three-dimensional accelerometer attached to a wheelchair.

The boundaries in ISO-2631 are based on cumulative root-mean-square (RMS) amplitude over a single day, specified for frequencies between 1 and 80 Hz. No allowance is made for the effect of recovery periods within a given day. There are three boundaries defined in

ISO-2631. These boundaries are, in increasing order of exposure: "reduced comfort boundary," the "fatigue-decreased performance boundary," and the "exposure limit boundary." The fatigue-decreased performance boundary is used as a baseline, and the other two boundaries are determined by direct scaling. The exposure limit boundary is defined to be 6 dB (two times) greater in magnitude than the fatigue-decreased performance boundary, and the reduced comfort boundary is defined as 10 dB less.

The resonant frequencies of the human body are used as the bases for determining the level of exposure allowed. The frequencies where the lowest longitudinal vibration exposure is allowed are in the range from 4 to 8 Hz, which is the resonant frequency range of the human body in the seated position. The boundaries for transverse vibration are lowest for the range of 1–2 Hz.


**Figure 1.**
SMART$^{ACC}$ properly mounted to the Quickie 2 wheelchair.

## SMART$^{ACC}$

The SMART$^{ACC}$ consists of a three-dimensional accelerometer mounted to the frame of a wheelchair, and a data logger (13). **Figure 1** is a photograph of the assembly. The three-dimensional accelerometer was mounted to align the axes of acceleration sensitivity with the axes of the wheelchair within 3º. The *z*-axis in this system is directed toward the right side of the wheelchair. The *x*-axis of the wheelchair-coordinate system is in the direction of wheelchair travel and the *y*-axis is upward. Either the *x*-axis or the *y*-axis of the accelerometer-coordinate system was aligned horizontally to within 3º of the *x*-axis of the wheelchair. For the two coordinate systems to be aligned, analysis software determined the proper orientation using gravitational acceleration when the wheelchair was at rest preceding the test.

A three-dimensional accelerometer with a suitable frequency range and accuracy was required for the SMART$^{ACC}$. Capacitive force-balance accelerometers from Analog Devices, Inc. (ADXL 05; Norwood, MA) were chosen because of the low power consumption, small size, low drift, and high linearity requirements of this study. These single-chip, force-balance accelerometers have a range of ±40 m/s$^2$ and the added capability of a built-in Butterworth, second-order, low-pass analog filter. For this study, a cutoff frequency of 100 Hz was set. Most vehicular dynamic measurements are made in the frequency band between direct current (DC, 0 Hz) to 50 Hz (14,15). Furthermore, it has been shown that the dynamic acceleration of a wheelchair being tested with the use of an ISO-ANSI/RESNA Double-Drum Test (DDT) or Curb-Drop Test (CDT) machine has a maximum frequency of approximately 25 Hz (1,2,16).

Each ADXL05 was supplied with a factory-certified calibration that was used for the study. The ADXL05 accelerometers have a maximum zero drift of ±100 mV. Since drift is a slow process, the effects of drift were removed, in this case, by simply extracting the DC component of the power spectral density (PSD) estimation. The ADXL05s have a nonlinearity of 0.2 percent, but a transverse sensitivity of up to 3.5 percent. The largest source for error is, therefore, the transverse sensitivity from mounting misalignment inside the module package.

## Bite-Bar Design

To determine a transfer function that represented the seated wheelchair user, acceleration at the head was measured. A bite bar provides a commonly used and convenient method to attach the accelerometer solidly to the head of the rider (3). This bite bar was formed from surgical stainless steel, as shown in **Figure 2**. Stainless surgical steel was chosen to provide an easily sterilized surface with good resistance to hydrochloric acid disinfectants. To provide a comfortable biting surface, two disposable polyurethane mouthpieces were used above and below the biting surface. The bite bar was held with the teeth between the mouthpieces with the accelerometer suspended 90º downward by the bite bar. The bite bar was sterilized in a bath of 10-percent common chlorine bleach for 10 min, as per the guidelines in the *Manual of Clinical Microbiology* (17).


**Figure 2.**
The nonsterilized accelerometer module of bite bar is external to the mouths of subjects.

The same ADXL05 accelerometer was used for both the SMART$^{ACC}$ and the bite bar. This three-dimensional accelerometer was kept external to the body at all times, since it could not withstand the sterilization procedures. The entire bite-bar assembly weighs 68 g.

### Subject Pool

The criteria for participation in this study were that individuals have a physical disability resulting in a mobility impairment and that they use a manual wheelchair for more than half of their individual mobility needs. No stratification was attempted concerning subject size or athleticism, as this study was intended to obtain a cross section of results applicable to wheelchair users in general and to evaluate potential testing procedures and standards. In all, sixteen subjects participated in the protocol. A list of characteristics of subjects is given in **Table 1**. These characteristics include the type and sizes of the wheelchairs and cushions used personally by the subjects, as well as the wheelchairs used in the testing.

### Simulated Road Course

A SRC was used to collect data from wheelchair users, over obstacles similar to those that are typically experienced by a wheelchair user (**Figure 3**) (18). The SRC consisted of eight obstacles fixed rigidly to a flat concrete surface. The first obstacle was a four-tile (4×16.5-cm) "truncated dome strip" guidance marker, usually used for visually impaired persons. The second obstacle was a piece of light-industrial carpet. Third was a simulated door threshold, 1.6 cm high, constructed of an aluminum plate (91.4 cm×25.4 cm). Fourth was a climb up a 1.27-m-long ramp leading to a 1.22-m$^2$ platform 5.0 cm off the floor, allowing the subject to attain level before traversing off a 5.0-cm drop. Fifth were two squares of "directional" guide strips (rumble bumps), also used for visually impaired persons. The sixth, seventh, and eighth obstacles were three sinusoidal bumps. Each was 91.4 cm×25.4 cm with the heights, in increasing order, of 2.5 cm, 5.1 cm, and 7.7 cm.

The SRC was repeated three times with an instrumented wheelchair at a freely chosen speed. Assistance with transferring was provided and a transfer board was available. Wheelchair selection was based on subject size, with choices being a Quickie 2 (Sunrise Medical Incorporated, Fresno, CA), a Kuschall 1000 (Kuschall of America, Camarillo, CA), or an E&J Metro (Everest & Jennings, St. Louis, MO). The tire pressures were set according to the recommendation of the manufacturer, before the testing began. The enclosure for the data loggers was placed in a book bag that was slung over the push handles of the test wheelchair with the SMART$^{ACC}$ mounted to the wheelchair frame. A sampling rate of 960 Hz, and an 8-bit A/D converter with a 5-V input range was used. This data logger has been described in detail previously by VanSickle (19).

During the entire test, a spotter followed the subject to prevent tipping and to keep the instrument cable from interfering with the subject's control of the wheelchair. Another investigator operated an IBM PC-compatible computer used for data collection. This individual pressed the space bar when the casters first touched the tape, indicating the beginning of an obstacle region, and when the rear wheels just cleared the tape, indicating the end of a task.

### Field Test

The field test began after the conclusion of the SRC test and the reprogramming of the data logger. For the field test, the bite bar was not used, to prevent inconvenience to the subjects. Each subject was given specific instructions on how to use the wheelchair, before the field test. The duration of the field test was a minimum of 4 h.

**Table 1.**
Subjects' characteristics.

| | Subject's wheelchair W (cm) × L (cm) | Diagnosis | Cushion type | Test wheelchair | Height (cm) | Mass (kg) |
|---|---|---|---|---|---|---|
| 1 | Quickie 2 38.1 × 38.1 | Spina bifida | Roho quattro | Kushall | 127 | 45 |
| 2 | Quickie rev. 45.7 × 45.7 | SCI | Contoured foam | Metro | 175 | 100 |
| 3 | E-Tack Swede elite 43.2 × 40.6 | SCI | Roho | Quickie 2 | 180 | 68 |
| 4 | Quickie 2 45.7 × 45.7 | SCI | Jay active | Metro | 183 | 100 |
| 5 | Quickie 2 40.6 × 40.6 | SCI | Flat foam | Metro | 180 | 95 |
| 6 | Quickie GPV 40.6 × 40.6 | SCI | Flat foam | Kushall | 183 | 80 |
| 7 | Quickie 2 43.2 × 45.7 | SCI | Jay | Quickie 2 | 183 | 82 |
| 8 | Invicare ridelite 40.6 × 40.6 | SCI | Jay | Kushall | 173 | 77 |
| 9 | Quickie 2 HP 35.6 × 40.6 | SCI | Roho (10 cm) | Kushall | 65 | 45 |
| 10 | Quickie GPV 40.6 × 40.6 | Multiple sclerosis | Flat foam | Quickie 2 | 196 | 77 |
| 11 | Quickie 2 45.7 × 45.7 | SCI | Roho (2.5 cm) | Quickie 2 | 173 | 91 |
| 12 | Quickie 2 40.6 × 43.2 | SCI | Roho (5 cm) | Quickie 2 | 170 | 75 |
| 13 | Quickie 2 45.7 × 35.6 | SSD* | Roho (10 cm) | Kushall | 173 | 45 |
| 14 | Action 45.7 × 43.2 | SCI | Jay | Quickie 2 | 183 | 80 |
| 15 | Quickie GP 43.2 × 55.6 | SCI | Jay | Kushall | 183 | 80 |
| 16 | Quickie 2 40.6 × 40.6 | SCI | Jay 2 | Kushall | 157 | 54 |

* Spastic spinal degeneration

Subjects were told to turn on the switch attached to the frame when they were in the wheelchair and turn it off when they transferred off the wheelchair (e.g., when driving a car). An LED provided visual feedback on the position of the switch to the subject. All subjects were instructed to use the wheelchair as they normally would and not to be concerned about the survivability of the instrumentation. Just as each subject was warned against being more timid than usual, each subject was also instructed not to try specifically to increase the aggressiveness of his or her activities. At the conclusion of the test, each subject was met at a predetermined location and the data uploaded to an IBM-PC laptop computer.

## Data Analysis

### *Spectral Analysis Using the Fast Fourier Transform*

Spectral analysis was performed with the periodogram technique, which is an estimation of the power spectral density based on the Discrete Fourier Transform (DFT). The SRC data were analyzed with a script written for MatLab (MathWorks, Inc., Natick, MA) while the field test data were analyzed with an algorithm written in C (Archimedes, Inc., Kirkland, WA) for the Motorola 68HC11A1 on the data logger described by VanSickle (13). The C program consisted of three interrupt-driven ring buffers, used to collect 8-bit conversions from the three acceleration directions; a high performance, radix-2 Fast Fourier Transform (FFT) algorithm; and an estimation of the cumulative PSD.

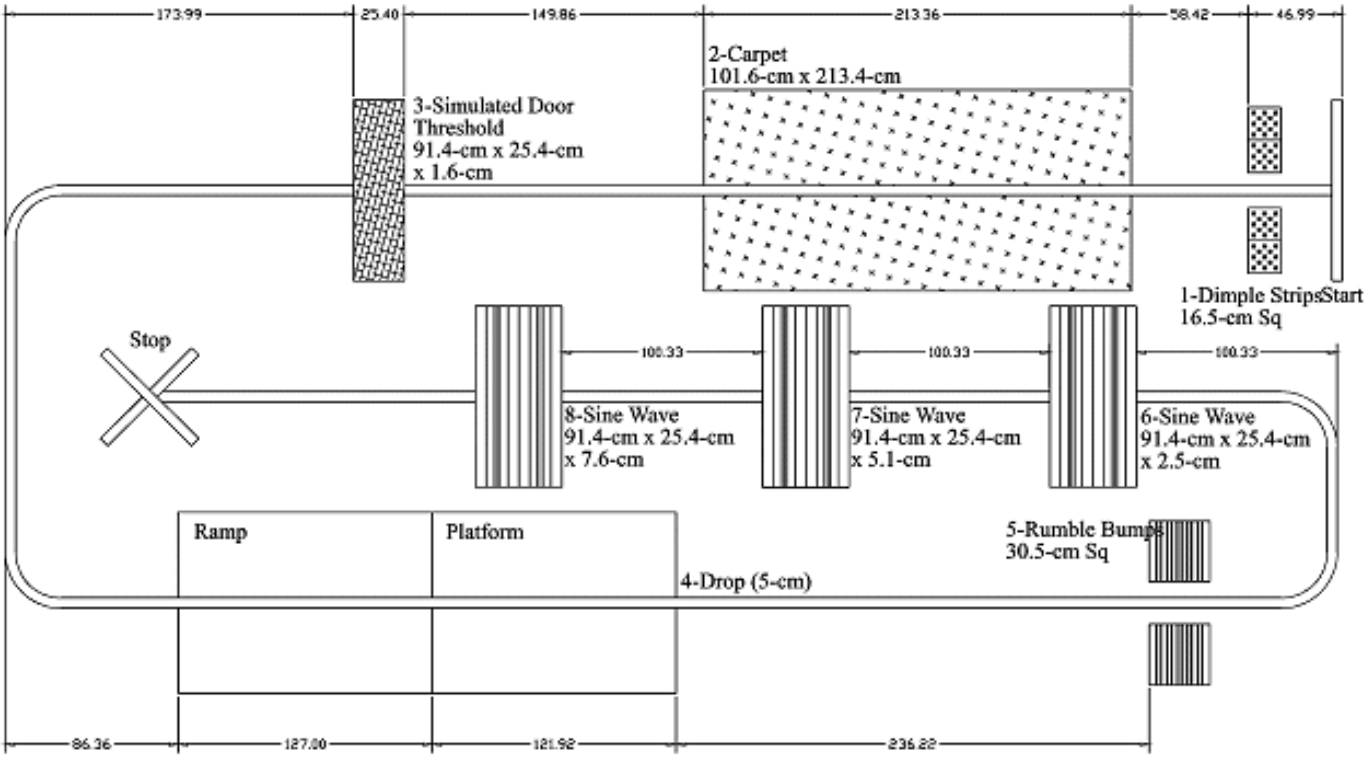


**Figure 3.**
Diagram of the Simulated Road Course (SRC) (units are in cm).

To improve performance, data from all three accelerations were transformed simultaneously inside the same looping structure. Furthermore, for each acceleration direction, two sequential 256-byte sequences were combined as complex data and calculated together. The first 256 bytes of each ring buffer ($f_k$) were treated as real input data, and the next 256 bytes ($g_k$) were treated as imaginary input data, as shown in Equation 1 (20).

$$h_k = f_k + jgk \qquad [1]$$

The discrete Fourier transform $F(\tilde{\omega})$ and $G(\tilde{\omega})$ can be separated from the discrete Fourier transform of the combined data by Equations 2 and 3, where l refers to the sampling frequency and the asterisk indicates the complex conjugate (20). Using this technique nearly doubles the speed of the FFT process.

$$F_l = \frac{H_l + H^*_{N-l}}{2} \qquad [2]$$

$$G_l = \frac{H_l - H^*_l}{2\,j} \qquad [3]$$

The PSD of each of the three acceleration signals is then estimated, with the use of Equation 4. $P_l$ is the signal power estimate, and N is the number of points in the FFT calculation (N=256). To reduce the storage requirements, the PSD estimates for frequencies of 1–14.8 Hz are stored in individual bins, but the PSD estimates from 15.6 to 83.6 Hz are grouped into bins of 3.125 Hz. In addition to estimating the average PSD, the program also calculates the maximum PSD for each of the frequency bins.

$$P_l = \frac{1}{N}\sum_{k=0}^{T}(F_{k,l})^2 + (G_{k,l})^2 + (F^*_{k,l})^2 + (G^*_{k,l})^2 \qquad [4]$$

Autoregressive moving-average (ARMA) modeling was used as a comparison to estimate the validity of the periodogram technique. With an ARMA model, the

measured data are assumed to be the impulse response of Equation 5. If all $a_i$ are zero, then the impulse response of Equation 5 is simply the DFT of $c_i$.

$$H(j\omega)=\frac{c_0+c_1e^{-j\omega t_0}+c_2e^{-2j\omega t_0}+\cdots+c_{(N-1)}e^{-(N-1)j\omega t_0}}{1+a_1e^{-j\omega t_0}+a_2e^{-2j\omega t_0}+\cdots+a_{(M-1)}e^{-(M-1)j\omega t_0}} \quad [5]$$

There are two fundamental approaches to the determination of the coefficients in the Yule-Walker equation corresponding to Equation 5. The coefficients can be determined simultaneously through use of linear programming techniques, or the AR coefficients can be determined first, followed by the MA coefficients. While the second technique is suboptimal, it was sufficient for determining the adequacy of the periodogram. (See Equation 6.)

$$x(k)+\sum_{n=1}^{p} a_n x(k-n)=\sum_{n=0}^{q} c_n \delta(k-n) \quad [6]$$

With the use of the suboptimal technique, all the coefficients of the MA model were set to zero, to form homogeneous Equation 7. The coefficients in Equation 7 can be determined directly by a least-squares technique if the order (p) of the AR model is known. One method of determining the order of an AR model is via the singular value decomposition (SVD) (21). For determining the adequacy of the periodogram, only the order needs to be determined, and not the actual coefficients.

$$x(k)+\sum_{n=1}^{p} a_n x(k-n)=0 \quad [7]$$

To use SVD, the autocorrelation matrix is formed with the use of an initial model order ($p_e$), selected to be larger than the expected AR model order in Equation 8. The autocorrelation matrix was then factored with an SVD algorithm based on QR iteration (22). This process determines the orthonormal square matrices, U and V, in Equation 9. The diagonal elements of the diagonal matrix, S, are the singular values.

$$\hat{R}=\begin{bmatrix} x_1 & x_2 & \cdots & x_{p_e} \\ x_2 & x_3 & \cdots & x_{(p_e+1)} \\ \vdots & & & \vdots \\ x_{(N-p_e)} & & & x_N \end{bmatrix}\begin{bmatrix} x_1 & x_2 & \cdots & x_{p_e} \\ x_2 & x_3 & \cdots & x_{(p_e+1)} \\ \vdots & & & \vdots \\ x_{(N-p_e)} & & & x_N \end{bmatrix} \quad [8]$$

$$R=U^{N\times N}(S^{N\times p_e})V^{p_e\times p_e} \quad [9]$$

Because the autocorrelation matrix is derived from experimental data, it is likely to be full rank, but the underlying AR process may not be. The singular values ($\sigma^2_i$) can be used to estimate the order of the underlying process using the ratio of the Frobenius norm of the reduced rank autocorrelation matrix ($\mathbf{R}^p$) to the Frobenius norm of the measured autocorrelation matrix ($\mathbf{R}$) as shown in Equation 10. The value of v(p) is dependent on the assumed order and converges to one as the p approaches $p_e$ or as the p approaches the true order of the system. In practice, the order is determined to be the minimum required such that v(p) is larger than an arbitrarily set threshold. For this study the threshold was set at 97 percent.

$$v(p)=\frac{\|\mathbf{R}^p\|}{\|\mathbf{R}\|}\left\{\frac{\sigma_1^2+\sigma_2^2+\cdots+\sigma_p^2}{\sigma_1^2+\sigma_2^2+\cdots+\sigma_{p_e}^2}\right\}^{1/2} \text{ where : } p\le p_e \quad [10]$$

*System Identification*

Two different methods for system identification were used to approximate a transfer function for acceleration from the wheelchair through the wheelchair user. The first method was based on the assumption that the input-output relationship can be modeled as a finite impulse response (FIR) filter with the use of the Wiener-Khintchine theorem, with the required assumption that the acceleration signal is wide sense stationary (WSS) and ergotic. The second method used the more general case of an autoregressive-autoregressive model with exogenous inputs (ARARX). Given input acceleration from the wheelchair frame and output acceleration from the mouth of the subject, the Wiener-Khintchine theorem was used to estimate the magnitude of the transfer function of the wheelchair/wheelchair-user system after the power spectral densities of the input and output accelerations are estimated from the DFT, as shown in Equation 11 (20).

$$|H(\omega)| = \sqrt{\frac{\hat{S}_{yy}(\omega)}{\hat{S}_{xx}(\omega)}} \qquad [11]$$

There are many methods of determining the parameters of an ARARX model that "best" fit the recorded input and output data. Most rely on a least-squares approach, but other methods use maximum likelihood techniques and even neural networks (23). The method used was a least-squares approach, where the output was assumed to be corrupted by colored noise (24). A diagram of this situation is shown in **Figure 4**.

In our case, the filter was an $r^{th}$-order AR function. With the use of a filter order equal to or higher than the AR portion of the transfer function H(z), a portion of the error may be assumed to be added to the input as well. Because the output of the model x(t) was not available, the colored noise v(t) was estimated.

The system in **Figure 4** is represented algebraically in the time domain by Equation 12 (24). This is a form of the Yule-Walker Equation with additive noise. The input of

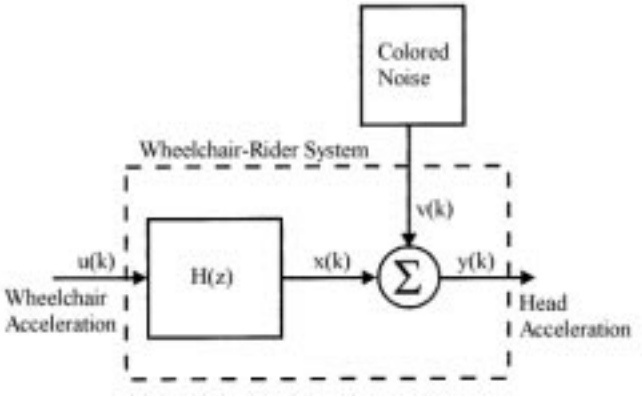


**Figure 4.**
Model of input-output relationship of acceleration signals. Measured output values, y(k), are assumed to be the result of input values (x(k)) coupled with convolution with the filter, H(z), and colored noise, v(k).

Equation 12 is the measured acceleration, u(k), and the noise, (v(k)), is colored by the AR model, defined by the coefficients $c_n$ in Equation 13. Equivalently, Equation 12 can be expressed in matrix terms as shown in Equation 14, and Equation 13 has a matrix equivalent as shown in Equation 15.

$$y(k) = \sum_{n=1}^{q} a_n u(k-n) - \sum_{n=1}^{p} b_n x(k-n) + v(k) \qquad [12]$$

$$v(k) = \sum_{n=1}^{r} c_n v(k-n) \qquad [13]$$

$$\mathbf{y} = \mathbf{A}\theta = \mathbf{v}$$

$$\mathbf{A} = \begin{bmatrix} u_k & u_{k-1} & \cdots & u_{k-m} & -x_{k-1} & -x_{k-2} & \cdots & -x_{k-n} \\ u_{k+1} & u_k & \cdots & & -x_k & -x_{k-1} & \cdots & -x_{k-n+1} \\ \vdots & \vdots & & & \vdots & \vdots & & \vdots \\ u_{k+p-1} & u_{k+p-2} & \cdots & u_{k+p-1} & -x_{k+p-2} & -x_{k+p-3} & \cdots & -x_{k+p-n-1} \end{bmatrix}$$

$$\theta = [a_0\ a_1 \ldots a_m\ b_1\ b_2 \ldots b^n]^T \qquad [14]$$

$$\mathbf{v} = \mathbf{B}\psi + \mathbf{z}$$

$$\mathbf{B} = \begin{bmatrix} v_{k-1} & v_{k-2} & \cdots & v_{k-r} \\ v_k & v_{k-1} & \cdots & v_{k+1-r} \\ \vdots & \vdots & & \vdots \\ v_{k+p-2} & v_{k+p-3} & \cdots & v_{k+p-r-1} \end{bmatrix}$$

$$\psi = [c_1\ c_2 \ldots c_r]^T \qquad [15]$$

The matrix **A** in Equation 13 is a concatenation of the current input and delayed inputs with delayed noiseless outputs x(k). Both the input AR and exogenous coefficients of the transfer function H(z) are contained within θ. The delayed noise values are arrayed in the matrix, **B**, and the coefficients of the AR noise model were given in the vector ψ Equation 15. The vector, **z**, was minimized by the least-squares process and represents the difference between the model of the noise and the actual additive noise. Equations 14 and 15 are combined into one matrix, Equation 16.

$$\mathbf{y}=[\mathbf{A}\ \mathbf{B}]\begin{bmatrix}\theta\\ \psi\end{bmatrix}+\mathbf{z} \qquad [16]$$

Because the input noise vector **v**(k) was not known *a priori*, an iterative approach was used. Solving Equation 16 for an estimate of θ gives Equation 17.

$$\hat{\theta}_i=(\mathbf{A}^T\mathbf{A})^{-1}\mathbf{A}\mathbf{y}-(\mathbf{A}^T\mathbf{A})^{-1}\mathbf{A}^T\mathbf{B}\hat{\psi}_{i-1} \qquad [17]$$

Similarly, solving Equation 16 for an estimate of ψ gives Equation 18. The subscript i indicates that this is the $i^{th}$ iteration of the estimate for θ.

$$\begin{gathered}\hat{\psi}_i=\mathbf{D}^{-1}\mathbf{B}^T\mathbf{M}\mathbf{y}\\ \mathbf{M}=\mathbf{I}-\mathbf{A}(\mathbf{A}^T\mathbf{A})^{-1}\mathbf{A}^T\\ \mathbf{D}=\mathbf{B}^T\mathbf{M}\mathbf{B}\end{gathered} \qquad [18]$$

As an initial condition, $\theta_0$ was estimated with the use of Equation 16 with the assumption that v(k) was zero. With use of Equation 15, v is calculated. $\psi_0$ is then estimated with Equation 18 and $\theta_1$ determined with Equation 17. The iteration is then continued until convergence in the estimate for the parameters θ was achieved. Convergence is assumed when the condition in Equation 19 is satisfied. A convergence error value of $10^{-4}$ was chosen.

$$\frac{(\theta_i-\theta_{i-1})^T(\theta_i-\theta_{i-1})}{(\theta_{i-1})^T\theta_{i-1}}<\varepsilon \qquad [19]$$

## RESULTS

### Acceleration Power Spectral Density Estimation

A typical PSD estimation graph for the field test is given in **Figure 5**, along with the 8-h "fatigue-decreased performance boundary" on a log scale (12). Both the average PSD estimates and the maximum PSD estimates are included. These maximum PSD estimates are the maximum power for 2.56 s at each frequency for the entire test. The time of 2.56 s corresponds to two sequential 256-point data series, analyzed together as a complex series with the use of an FFT.

**Figure 6** displays the PSD estimates from the SRC. The maximum PSD was not estimated for this in-lab testing because the nonreduced data were available, unlike for the field test. **Figure 6** displays the PSD estimates from the SMART$^{ACC}$ and the bite bar. In addition to estimating the PSD with the FFT method, singular value decomposition was performed to determine if the FFT model would be sufficient for this analysis. For all cases, the autoregressive component of the signal was determined to be of zero order (24). Therefore, using the FFT to estimate the PSD is adequate (20,21). This provides additional confidence that the use of the FFT for real-time PSD estimation on the data logger during the field test was also valid.

**Figure 7** presents graphs of transfer functions between the SMART$^{ACC}$ and the bite bar. These transfer functions were derived for all 16 subjects who participated in this study. Data from the rumble bumps portions of the SRC was used for the derivation of the transfer function because this section produced the richest signal (most varied frequency content) as determined from the examination of PSD estimates. The graphs show the transfer functions derived with the use of both frequency division and the ARARX model. The anterior-posterior acceleration transfer functions and the lateral acceleration transfer functions did not show peaks consistently.

## DISCUSSION

A main thrust of this study was aimed at understanding wheelchair-rider comfort as it relates to vibration exposure. This approach was chosen because of the large quantity of literature that has been accumulated regarding vibration exposure and the link to neck pain (25), low-back pain (26–28), and abdominal and stomach discomfort (29).

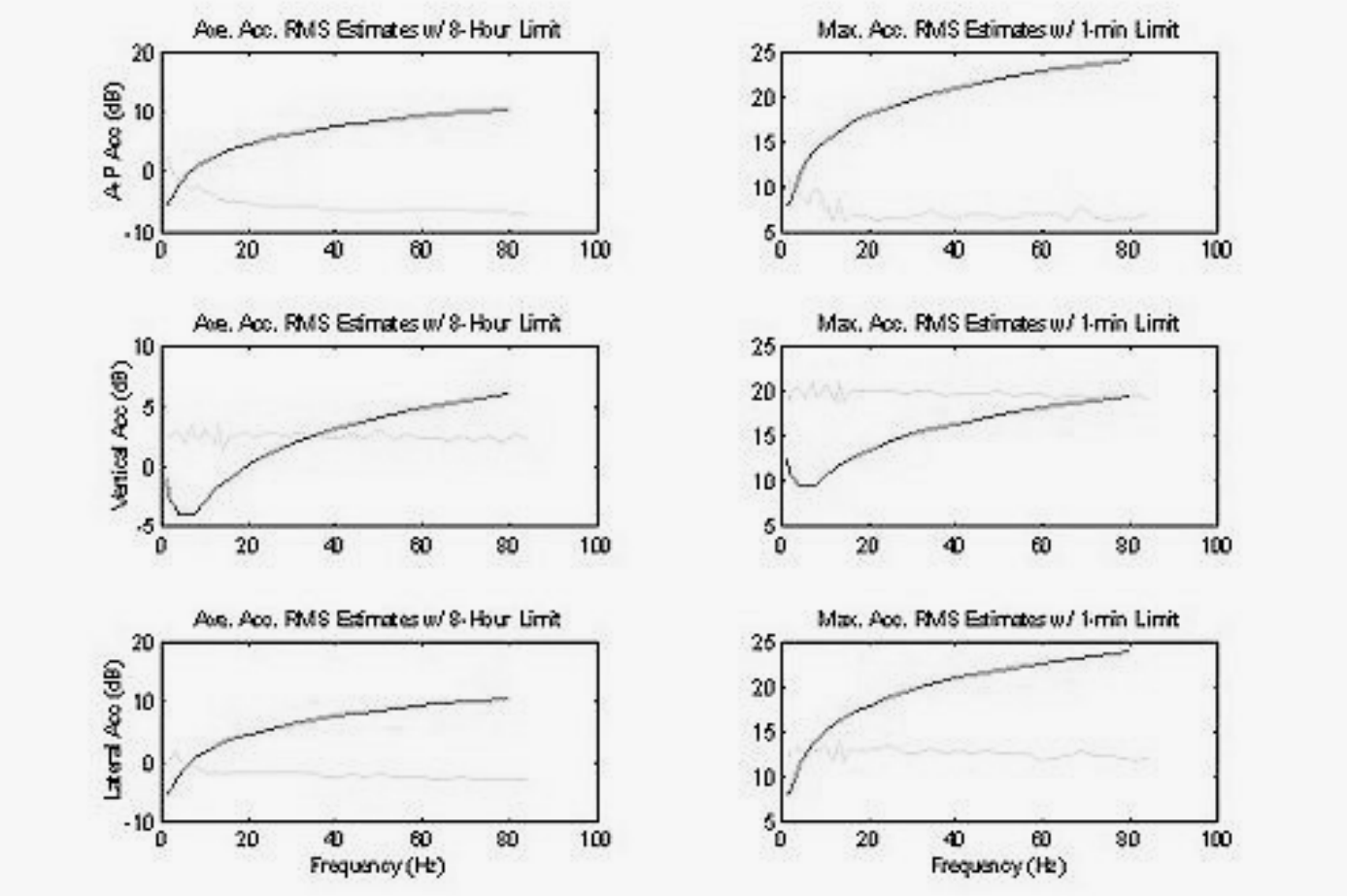


**Figure 5.**
Power spectral density estimations during the field test, using the FFT technique. Left Column: Cumulative PSD estimates shown for the 8-h, ISO-2631, fatigue-decreased proficiency boundary (A-P, vertical, and lateral accelerations, respectively). Right Column: Peak PSD estimates shown for the 1-min, ISO-2631, fatigue-decreased proficiency boundary (A-P, vertical, and lateral accelerations, respectively).

It is clear from the results that for the SRC course, the acceleration at the wheelchair frame exceeds the 8-h "fatigue-decreased performance boundary" (12). Furthermore, the acceleration at the head exceeds the same boundary. It could be argued that the cushion absorbed some of the acceleration measured at the frame and did not transmit the full magnitude to the subjects. If the acceleration at the head exceeds the ISO-2631 boundaries, it is likely that the acceleration transmitted through the wheelchair cushion exceeds the boundaries as well. Further studies will be needed to evaluate the effect of cushions on the dynamics of a wheelchair rider. Unfortunately, a standardized cushion cannot be used, because the subject's own cushion is necessary to prevent potential ischemic injury.

Using transfer functions to compare the accelerations at the head with those at the wheelchair demonstrated that there was considerable dampening beyond approximately 20 Hz. This dampening was probably due to vibration absorption by the bodies of subjects. Heavy dampening for this range of frequencies is consistent with the literature (3,30,31). The short data sets over the "rumble strips" have the disadvantage of limiting the usefulness of the frequency division methodology for determining the transfer function between the SMART$^{ACC}$ and the bite bar.

The variance of the transfer function derived with the frequency-division method is inversely proportional to the number of individual PSD estimates used for the average PSD of the input and output acceleration signals (20,24). A vertical acceleration resonant peak was evident for eight of the subjects. The average for these peaks, when present, was 8.1 Hz. This frequency is higher than the 4–6 Hz resonant peak presented in the literature for a

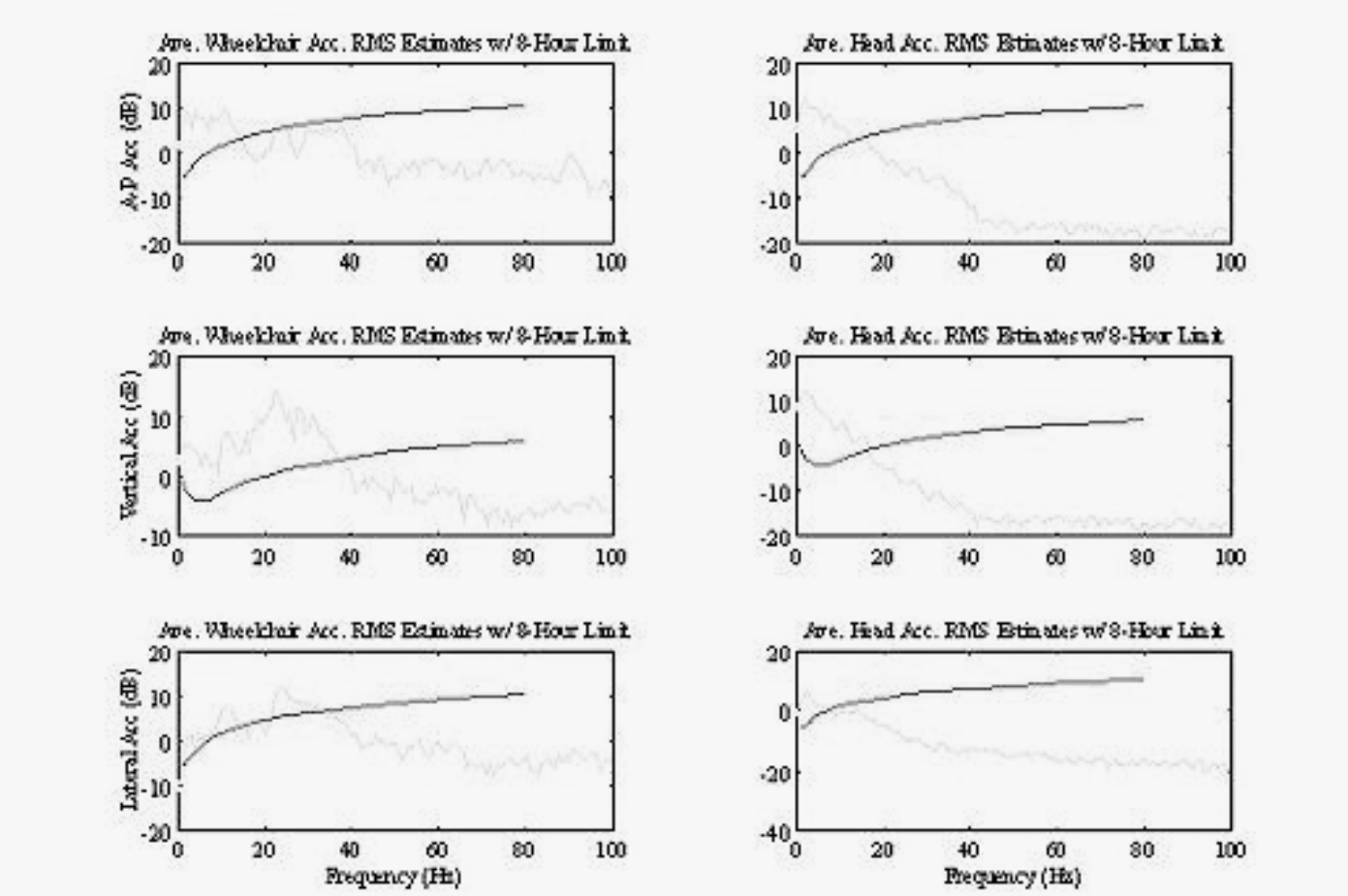


**Figure 6.**
Power spectral density estimation during the simulated road course, using the FFT-based periodogram technique. Left Column: Average PSD estimates for A-P, vertical, and lateral accelerations, respectively, at the wheelchair frame. Right Column: Average PSD estimates for A-P, vertical, and lateral accelerations, respectively, at the bite bar.

seated human subject (3,30,31). The difference between the measured resonant peak and the literature values may be related to a feature of the seating position inherent to wheelchair propulsion, or may be related to the population tested. This study used only subjects with disabilities, many of whom had spinal cord injuries or other musculature deficits. According to Seidel, the resonant peak may be influenced by active muscle control (3,30). For one to further analyze this result, it would be desirable to modify the SRC to include a much longer section of the "rumble bumps" to provide a more accurate estimation of the transfer function, with the use of either the frequency division or the ARARX method.

During the field test, the anterior-posterior acceleration ($a_x$) and the lateral acceleration ($a_y$) PSDs crossed the "fatigue-decreased performance boundary" only at the lowest frequencies. This appears to be due to voluntary motion of the user while propelling the wheelchair. Evidence for this assumption comes from knowledge of how individuals use their wheelchairs and from the maximum PSD estimation. The maximum PSD estimation for the anterior-posterior acceleration was only slightly greater than the average PSD estimation, indicating that the acceleration amplitude must be repetitive in nature and occur nearly continuously throughout the day, consistent with wheelchair propulsion. Wheelchair propulsion, however, usually occurs at a rate of approximately 1 Hz. The average PSD graphs show an increase from 1 Hz (lowest frequency measured) to approximately 8 Hz. This was probably due to two factors. There was likely some "leakage" of the acceleration signal power from the 1-Hz bin to the higher frequencies, simply

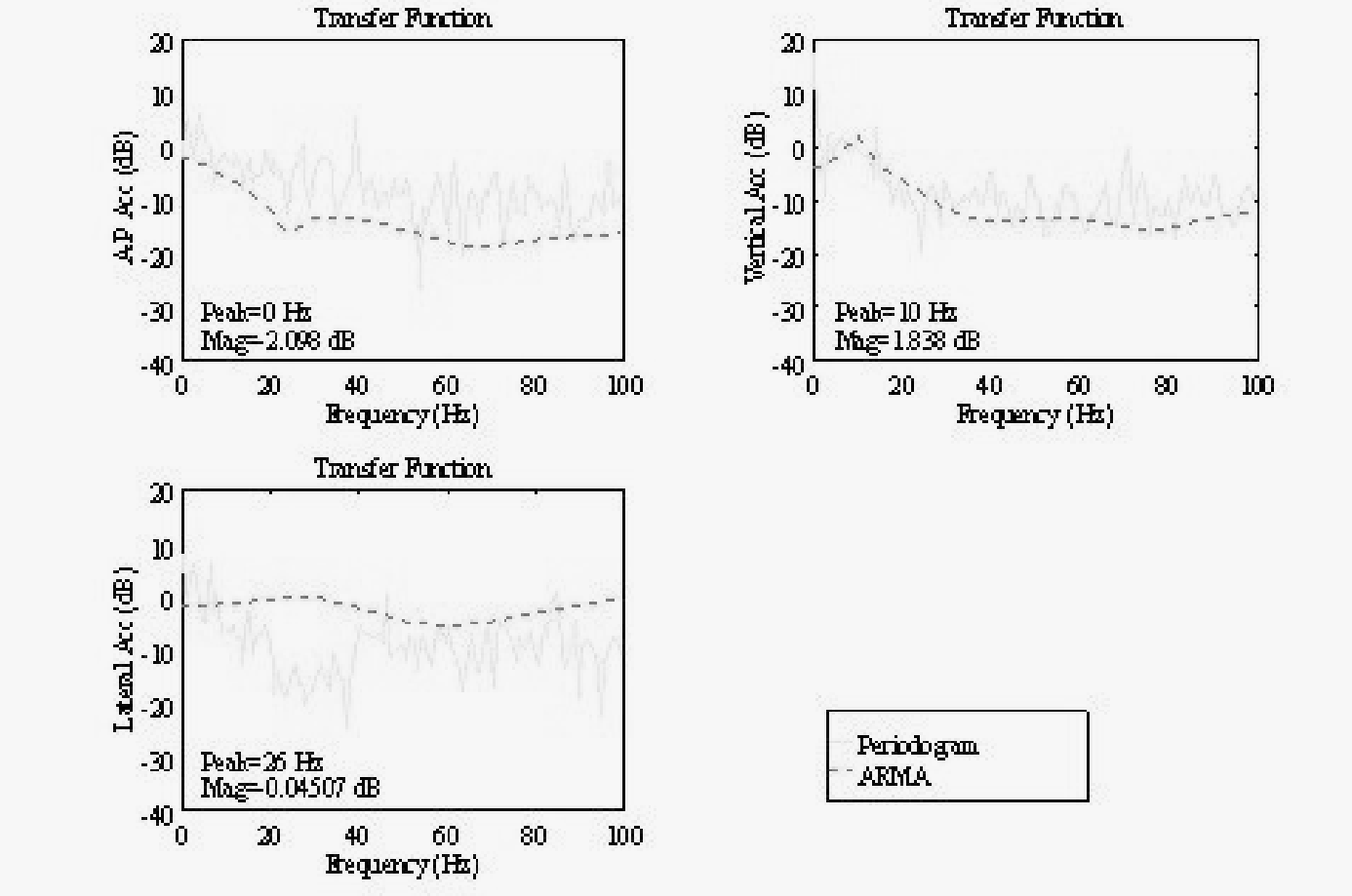


**Figure 7.**
Power spectral density estimates during the rumble bumps of the simulated road course. The periodogram technique is used with the rational model (MA order=6, AR order=5, AR noise order=3), to provide estimates of A-P, lateral, and vertical accelerations.

because of the numerical calculation of the FFT. Because this leakage was at most 4 percent from the most significant frequency to its nearest neighbor, this was likely a minor contributor. The major contributor to these higher frequencies is likely the higher-frequency components of the propulsion activity.

Unlike the anterior-posterior acceleration, the vertical acceleration greatly exceeded the limit defined by the 8-h "fatigue-decreased performance boundary." For this case, the maximum PSD profile was similar to the average PSD profile, but the magnitude of the maximum PSD was much greater. The most likely explanation is that the subjects and their wheelchairs were exposed to a few high acceleration events rather than consistent, small-magnitude accelerations. If true, this is a case where the ISO-2631 standard applies only tangentially (12). The standard states that all accelerations of 1-min duration or less must be smaller in magnitude than the 1-min boundary, and this boundary is clearly exceeded. The problem with using frequency analysis for an impulse signal is that very high-speed sampling is necessary to capture an accurate picture of the impulse. Such high sampling rates would require faster processing than was available for this study. Another type of analysis may provide more information about the accelerations experienced by wheelchair users. An algorithm that detects acceleration peaks and records the acceleration magnitudes might be more appropriate for this application. Rainflow analysis may be an even better choice, because it includes the same information as a peak detection method and is simpler to implement.

In addition to peak detection algorithms, wavelet analysis may work well (32). In simple terms, wavelet analysis is a hybrid between frequency analysis and time-domain analysis, with localization in both time and frequency. Frequency analysis provides a poor localization in time by averaging the results over the entire Fourier transform period. The ISO-2631 standard assumes that

the subject will be exposed to a constant or near-constant level of vibration exposure over the timeframe of the test. This does not appear to be the case for wheelchair users, because data point to exposure to large impulsive accelerations that occur infrequently throughout the day. This mandates the development of a different test methodology for acceleration measurement.

## REFERENCES

1. VanSickle DP, Cooper RA. Demonstration of a methodology for wheelchair acceleration analysis. In: Proceedings of the 15th Annual International Conference of the IEEE-Engineering in Medicine and Biology Society; 1993 Oct 28–31; San Diego, CA. Piscataway, NJ: Institute of Electrical and Electronic Engineers; 1993. p. 1301–2.
2. VanSickle DP, Cooper RA, Robertson RN. A 2-dimensional wheelchair dynamic load history using accelerometers. In: Proceedings of the RESNA '93 Annual Conference; 1993 June 12–17; Las Vegas, NV. Arlington, VA: RESNA; 1993. p. 324–6.
3. Seidel H, Bluethner R, Hinz B. Effects of sinusoidal whole-body vibration on the lumbar spine: the stress-strain relationship. Int Arch Occup Environ Health 1986;57(3):207–23.
4. Seroussi RE, Wilder DG, Pope MH. Trunk muscle electromyography and whole body vibration. J Biomech 1989;22(3):219–29.
5. Dupuis H. Biodynamic behavior of the trunk and the abdomen during whole-body vibration. Acta Anaesthesiol Scand 1989; Suppl(Feb):34–8.
6. Fairley TE, Griffin MJ. The apparent mass of the seated human body: vertical vibration. J Biomech 1989;22(2):81–94.
7. Muksian R, Nash Jr CD. A model for response of seated humans to sinusoidal displacements of the seat. J Biomech 1974;7(3):209–15.
8. Muksian R, Nash Jr CD. On frequency-dependent dampening coefficients in lumped-parameter models of human beings. J Biomech 1976;9(5):339–42.
9. Amirouche FML. Modeling of human reactions to whole-body vibration. J Biomech Eng 1987;109(3):210–7.
10. Amirouche F, Xie M, Patwardhan A. Optimization of the contact damping and stiffness coefficients to minimize human body vibration. J Biomech Eng 1994;116(4):413–20.
11. International Organization for Standardization, ISO 2631-3. Evaluation of human exposure to whole-body vibration. Part 3: evaluation of exposure to whole-body *z*-axis vertical vibration in the frequency range 0.1 to 0.63 Hz. Washington, DC: ANSI Press; 1985.
12. International Organization for Standardization, ISO 2631-1. Evaluation of human exposure to whole-body vibration. Part 1: general requirements. Washington, DC: ANSI Press; 1985.
13. VanSickle DP, Cooper RA, Gonzalez J. SMARTACCELEROMETER: a device to measure three-axis acceleration for the purpose of evaluating wheelchair rider comfort. In: Proceedings of the RESNA '97 Annual Conference; 1997 June 20–24; Pittsburgh, PA. Arlington, VA: RESNA; 1997. p. 245–7.
14. Nwagboso CO. Road vehicle automation. NY: Chapman and Hill; 1990. p. 125–40.
15. Sulouff REJ. Silicon sensors for automotive applications. In: International Conference on Solid State Sensors and Actuators; 1991 June 7–10; San Francisco, CA. Piscataway, NJ: IEEE Service Center; 1991. p. 170–6.
16. VanSickle DP, Cooper RA. Experimental determination of stress distribution due to wheelchair dynamic loads for use with finite elements. In: Proceedings of the RESNA '94 Annual Conference; 1994 June 17–24; Nashville, TN. Arlington, VA: RESNA; 1994. p. 575–7.
17. Rutala WA. Manual of clinical microbiology. Antisepsis, disinfection and sterilization in hospitals and related institutions. Washington DC: ASM Press; 1996. p. 227–45.
18. DiGiovine MM, Cooper RA, Boninger ML, Lawrence BL, VanSickle DP, Rentschler DJ. User assessment of manual wheelchair ride comfort and ergonomics. Arch Phys Med Rehabil 2000;81:112–7.
19. VanSickle DP. Realistic road loads and rider comfort for manual wheelchairs [doctoral dissertation]. Pittsburgh, PA: University of Pittsburgh; 1998.
20. Roberts RA, Mullis CT. Digital signal processing. Reading, MA: Addison-Wesley Publishing Company; 1987. p. 85–550.
21. Oppenheim AV, Schafer RW. Discrete-time signal processing. Englewood Cliffs, NJ: Prentice Hall; 1997. p. 514–642.
22. James ML, Smith GM, Wolford JC. Applied numerical methods for digital computation. 3rd ed; New York, NY: Harper and Row; 1985. p. 147–289.
23. Chon KH, Cohen RJ. Linear and nonlinear ARMA model parameter estimation using an artificial neural network. IEEE Trans Biomed Eng 1997;44(3):168–74.
24. Sinha NK, Kustzta B. Modeling and identification of dynamic systems. New York, NY: Van Nostrand Reinhold Company; 1983. p. 27–50.
25. Viikari-Juntura E, Riihimaki H, Tola S, Videman T, Mutanen P. Neck trouble in machine operating, dynamic physical work and sedentary work: a prospective study on occupational and individual risk factors. J Clin Epidemiol 1994;47(12):1411–22.
26. Hulshof C, van Zanten BV. Whole-body vibration and low-back pain. A review of epidemiologic studies. Int Arch Occup Environ Health 1987;59(3):205–20.
27. Pope MH, Hansson TH. Vibration of the spine and low back pain. Clin Orthop 1992;279(Jan):49–59.
28. Dupuis H, Zerlett G. Whole-body vibration and disorders of the spine. Int Arch Occup Environ Health 1987;59(4):323–36.
29. Kjellberg A. Psychological aspects of occupational vibration. Scand J Work Environ Health 1990;16 Suppl 1:39–43.
30. Seidel H, Harazin B, Pavlas K, Sroka C, Richter J, Bluthner R, et al. Isolated and combined effects of prolonged exposures to noise and whole-body vibration on hearing, vision and strain. Int Arch Occup Environ Health 1988;61(1–2):95–106.
31. Seidel H, Heide R. Long-term effects of whole-body vibration: a critical survey of the literature. Int Arch Occup Environ Health 1986;58(1):1–26.
32. Provaznik I, Kozumplik J. Wavelet transform in electrocardiography-data compression. Int J Med Informatics 1997; 45(1–2):111–28.

Submitted for publication February 17, 2000. Accepted in revised form June 12, 2000.